DOI: 10.1002/ejic.200800560

Aerobic Fe^{III}–Fe^{II} Reduction in the Presence of 2,4,6-Tri(2-pyridyl)-1,3,5-triazine and Benzilic Acid: Synthesis and Characterization of a Heptacoordinate Fe^{II}–Nitrato Complex

Catherine P. Raptopoulou,*[a] Yiannis Sanakis,[a] and Athanassios K. Boudalis[a]

Keywords: Aerobic reduction / Iron / N ligands / Moessbauer spectroscopy

The simultaneous presence of benzilic acid [$Ph_2C(OH)CO_2H$] and tptz [2,4,6-tri(2-pyridyl)-1,3,5-triazine] in Fe^{III}-containing reaction mixtures leads to partial and/or quantitative metal reduction. In the presence of the oxidative NO_3^- ions in the reaction mixture, partial reduction of the metal leads to the isolation of a heptacoordinate Fe^{II}–nitrato complex, [Fe^{II}(tptz)-$(NO_3)(MeOH)_2$](NO_3) (**1**), along with a Fe^{III} complex (**2**). In the presence of perchlorate ions in the reaction mixture, the quantitative reduction of Fe^{III} leads to the isolation of a hexacoordinate Fe^{II} complex, [Fe^{II}(tptzH)$_2$]$(ClO_4)_4$ (**3**). Complexes **1** and **3** have been structurally characterized and possess a pentagonal-bipyramidal and a distorted octahedral coordination geometry, respectively. In both complexes, tptz behaves as a tridentate ligand, adopting the terpy-like coordination mode, and is coordinated through the triazine nitrogen atom and the two adjacent pyridine nitrogen atoms. One asymmetrically coordinated chelate, NO_3^-, and two MeOH molecules complete the pentagonal-bipyramidal geometry around Fe^{II} in **1**. On the basis of analytical, spectroscopic (IR, Mössbauer) and magnetic susceptibility data from polycrystalline samples of **2**, an oxido-bridged diferric structure is proposed [ΔE_Q(78 K) = 1.79 mm s^{-1}, J_{Fe-Fe} = –117 cm^{-1}]. The Mössbauer spectra of the polycrystalline samples of **1** and **3** are consistent with high-spin and low-spin Fe^{II}, respectively, in an N/O coordination environment. Variable-temperature and variable-field magnetic measurements of **1** suggest significant zero-field splitting of the ferrous ions (D = 5.5 cm^{-1}).

Introduction

The coordination chemistry of tptz [2,4,6-tri-(2-pyridyl)-1,3,5-triazine] has drawn much attention in supramolecular and analytical chemistry. In particular, tptz is a neutral multifunctional N-donor ligand that: (i) can simultaneously function as a bidentate and a tridentate agent and therefore can be used as a potential spacer in the design of supramolecular complexes;[1] (ii) contains large π systems, which are determinative for the stabilization of the supramolecular structures;[2] (iii) is widely used as an analytical reagent for a variety of metal ions;[3] and (iv) can extract actinides from lanthanides in strongly acidic media, which is of potential interest in nuclear fuel reprocessing.[4]

A schematic drawing of the binding sites of the tptz ligand is depicted in Scheme 1. Most often, tptz acts as a tridentate ligand, adopting the terpy-like binding mode **I**, which usually leads to mononuclear complexes.[5,6] Only a few examples of tptz complexes showing the bidentate bpy-like binding mode **II** have been reported,[1b,7–9] while there are limited examples of complexes in which the tptz ligand acts simultaneously as a chelating and bridging ligand, either by adopting coordination mode **III**[1a,10–11] or **IV**.[7] The potential tris(bidentate) bpy-like binding mode **V** of tptz has not been observed so far.

Our interest in the coordination chemistry of tptz is related to our research on the carboxylate chemistry of the 3d metal ions in the presence of neutral N-donor ligands. Within this context, we had previously investigated the iron(III) chemistry of bidentate N-donor ligands in the presence of various carboxylates;[12] our research also includes the study of copper(II) complexes with bi- and tridentate N-donor ligands in the presence of dicarboxylates and/or their monoamides.[13] We thought that the use of a tridentate imine base, like tptz, in combination with carboxylate ligands, might lead to polynuclear clusters of iron(III) with new structural types, because of the constraint imposed by the ligand to coordinate equatorially to the metal ions. With this in mind, we decided to study the Fe^{III}/tptz/$Ph_2C(OH)CO_2H$ reaction system, which, unexpectedly led to unusual behavior. Herein, we report on the isolation of the first heptacoordinate Fe^{II}–nitrato complex [Fe^{II}(tptz)-$(NO_3)(MeOH)_2$](NO_3) (**1**) and the octahedral complex [Fe^{II}(tptzH)$_2$]$(ClO_4)_4$ (**3**) that contains the protonated form of tptz. The role of benzilic acid in the aerobic metal-ion reduction is also examined.

[a] Institute of Materials Science, NCSR "Demokritos", 15310 Aghia Paraskevi, Athens, Greece
Fax: +32-10-6519430
E-mail: craptop@ims.demokritos.gr

Supporting information for this article is available on the WWW under http://www.eurjic.org or from the author.

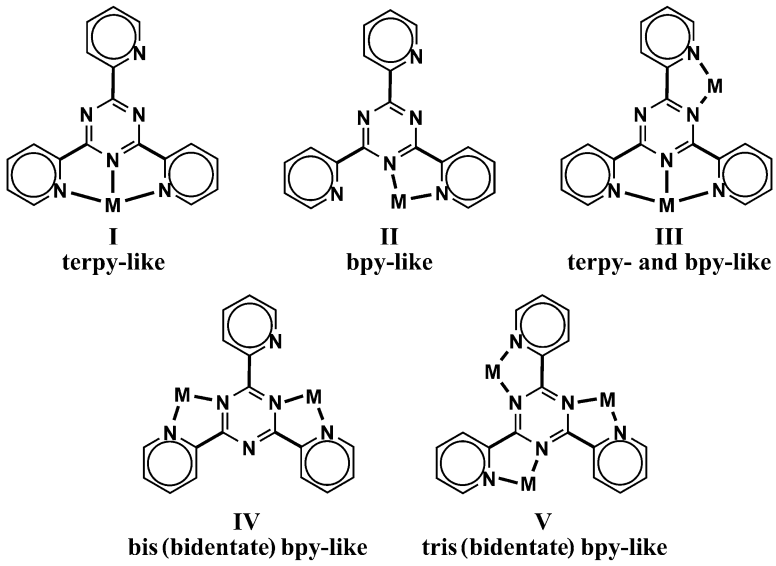

Scheme 1. The crystallographically established (**I**–**IV**) and the potential (**V**) binding modes of the tptz ligand.

Results and Discussion

Syntheses of the Complexes

The reaction of 1 equiv. $Fe(NO_3)_3·9H_2O$ with 2 equiv. $Ph_2C(OH)CO_2H$ in MeOH afforded a red solution, which immediately changed to deep purple on addition of 1 equiv. tptz (Scheme 2). Over a period of 30 min whilst stirring at room temperature, an orange powder (**2a**) formed, which was filtered off, and vapour diffusion of Et_2O to the deep purple filtrate afforded blue crystals of $[Fe^{II}(tptz)(NO_3)(MeOH)_2](NO_3)$ (**1**). The stabilization of the +2 oxidation state of the iron in **1** is remarkable given the presence of the oxidative NO_3^- ions in the reaction mixture, and more so, because of the fact that **1** is stable in air for prolonged periods of time, as evidenced by the retention of its crystal shape, colour, and IR spectroscopic features. To the best of our knowledge, from the structurally characterized Fe^{II}–nitrato complexes reported so far,[14,15] only one was synthesized under aerobic conditions.[15] Its formation was the result of the concomitant oxidation of the ligand *N*,*N*′-bis(2-pyridyl)urea. In addition, **1** represents the first example of a heptacoordinate Fe^{II}–nitrato complex. The orange powder (**2a**) was characterized as an oxido-bridged Fe^{III}_2 complex by microanalytical, spectroscopic (IR, Mössbauer) and magnetic susceptibility data (vide infra).

In order to verify the key factors leading to the nonquantitative reduction of the Fe^{III} ions and the unanticipated isolation of **1** from the above reaction mixture, we have carried out certain "blind" experiments. Our first attempt involved the reaction of 1 equiv. $Fe(NO_3)_3·9H_2O$ with 1 equiv. tptz in MeOH, i.e. elimination of benzilic acid from the reaction mixture, which afforded a red solution whose colour changed to blue after half an hour of stirring at room temperature. During that time, an orange powder (**2b**) formed with identical microanalytical and spectroscopic features (IR, Mössbauer) as compound **2a**, but no crystals of **1** formed. Vapour diffusion of Et_2O to the blue solution yielded only an orange precipitate, followed by decolourization of the solution. We thus assume that the blue filtrate initially contains a reduced Fe^{II} complex, which could not be stabilized in the absence of benzilic acid and re-oxidizes to the ferric complex **2**, i.e. the presence of only tptz in the reaction mixture is insufficient for the stabilization of the +2 oxidation state of the iron.

Our next attempt involved the reaction of 1 equiv. $Fe(NO_3)_3·9H_2O$ with 2 equiv. benzilic acid in MeOH, i.e. elimination of tptz from the reaction mixture. We had previously investigated the above-mentioned reaction system and had isolated orange crystals of the "basic iron(III) benzilate" complex, $[Fe_3O\{O_2CC(OH)Ph_2\}_6(MeOH)_2(H_2O)](NO_3)$,[16] and yellow crystals of the dodecanuclear "ferric wheel" compound, $[Fe(OMe)_2\{O_2CC(OH)Ph_2\}]_{12}$[17] upon addition of $LiOH·H_2O$. No signs of metal reduction were observed in any of those cases. Thus, there is no direct evidence that benzilic acid can serve as a reducing agent by itself.

We also examined the role of the reaction medium, by employing analogous reactions in MeCN (these procedures are not described in the Experimental Section). In the presence of benzilic acid, mixtures of blue and orange microcrystalline products were obtained, which could not be separated for further characterization; in the absence of benzilic acid, only an orange precipitate formed (Scheme 2). On the basis of the colours of the products, we conclude that the same redox processes occur in both methanol and acetonitrile solutions.

In order to verify the role of the oxidative and chelating NO_3^- ions, we also used iron(III) perchlorate as starting material, since perchlorates are neither oxidative nor chelating. Similarly, in order to ascertain the role of benzilic acid, the reaction system was studied both in its presence and absence. Thus, the reaction of 1 equiv. $Fe(ClO_4)_3·9H_2O$ with 2 equiv. $Ph_2C(OH)CO_2H$ afforded a red solution, which

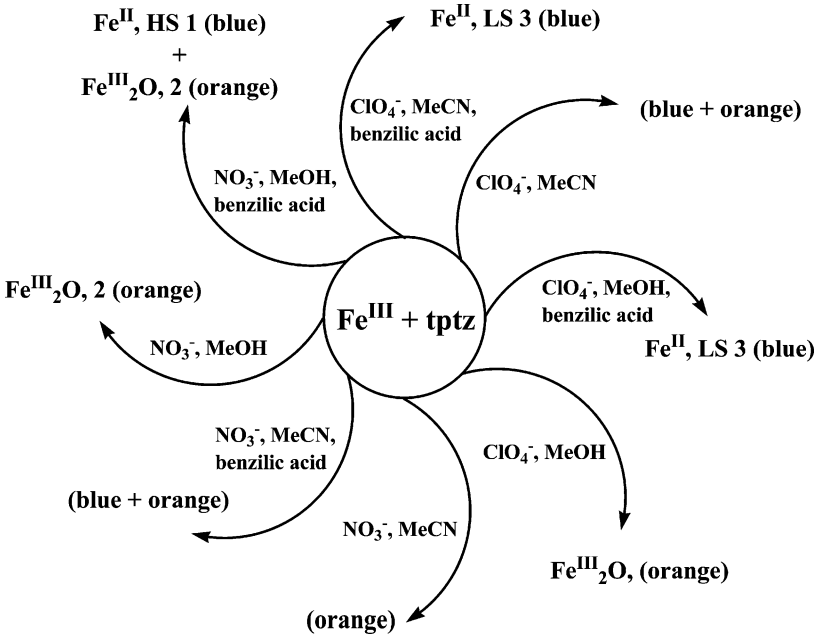

Scheme 2. The synthetic procedures discussed in the text.

changed to deep blue after the addition of 1 equiv. tptz and subsequent heating to reflux for 10 min or stirring at room temperature for 30 min. Slow evaporation of the reaction solvents yielded only blue crystals of $[Fe^{II}(tptzH)_2](ClO_4)_4$ (**3**), which are stable in air for prolonged periods of time, as evidenced by the retention of their crystal shape, colour, and IR spectroscopic features. On the other hand, elimination of benzilic acid from the above reaction system (this procedure is not described in the Experimental Section) yielded mixtures of an orange powder and a blue microcrystalline product, which could not be separated for further characterization.

We also examined the role of the reaction medium on the products of the $Fe(ClO_4)_3{\cdot}9H_2O$/tptz reaction mixtures both in the presence and absence of benzilic acid. Reactions in MeOH solutions revealed that in the absence of benzilic acid (this procedure is not described in the Experimental Section), an orange precipitate formed, whose microanalytical and spectroscopic (IR, Mössbauer) data suggest mainly an oxido-bridged diferric complex (Scheme 2, Figure S1a); in the presence of benzilic acid, a deep-blue precipitate formed, whose microanalytical and spectroscopic (IR, Mössbauer) data are identical to that of complex **3** (see Experimental Section, Method B, Scheme 2, Figure S1b).[18] The synthetic procedures discussed above are depicted in Scheme 2.

We are uncertain of the exact reaction mechanisms and pathways that lead to the aerobic reduction of Fe^{III} to Fe^{II} and the isolation of the ferrous complexes **1** and **3** from the above reaction mixtures. Without any mechanistic implication, we suggest that both benzilic acid and tptz are necessary for the aerobic reduction process on the basis of the following: (i) Benzilic acid is known to undergo oxidative decarboxylation to benzophenone, $Ph_2C{=}O$, in the presence of various oxidants.[19] The reverse reaction has also been reported to occur electrolytically,[20] which leads to electrocarboxylation of benzophenone to benzilic acid. However, oxidation to another product cannot be precluded. (ii) The reduction from ferric to ferrous ions is also known to be facilitated by the coordination of imines. The presence of these electron-withdrawing groups raises the reduction potential of the $Fe^{III} + e^- \rightleftarrows Fe^{II}$ redox couple, which renders the reduction product thermodynamically more stable.[21] This stabilization of the reduced species by imine ligands has previously led to the reduction of Fe^{III} to Fe^{II} by the solvent and/or ligand, even under aerobic conditions, and to ferrous products stable to oxidation.[15,22] Although there is no direct evidence, we suggest that tptz, like phen,[21] increases the reduction potential of the Fe(II)/Fe(III) redox couple, sufficiently for the benzilic acid to reduce the putative $[Fe(tptz)(MeOH)_x(NO_3)_y]^{(3-y)+}$ ($x = 2$ or 3; $y = 0$ or 1) and $[Fe(tptz)_2]^{3+}$ species to the corresponding ferrous species, which lead to complexes **1** and **3**, respectively. Particularly for **1**, we are uncertain of the nature of the intermediate ferric species and whether the complexation of nitrates occurs before or after reduction. However, we observe that elimination of nitrates leads to the quantitative reduction of Fe^{III} to Fe^{II}.

Compounds **1** and **3** have been structurally characterized, whereas compounds **2a** and **2b** have both been formulated as "$[Fe^{III}_2O(tptzH)_2(H_2O)_4](NO_3)_6{\cdot}2H_2O$" on the basis of their analytical, spectroscopic (IR, Mössbauer) and magnetic susceptibility data (vide infra).

IR Spectroscopy

In the IR spectra of **1**–**3**, the characteristic bands of tptz are observed as a set of peaks in the 1600–1200 cm^{-1} region,

which can be attributed to the ν(C=C) and ν(C=N) stretching vibrations of the pyridine and triazine rings of the ligand.[23] In the spectra of **1**, and in the same region, the bands expected for the crystallographically established chelating bidentate NO_3^- ion [$\nu_1(A_1) \approx 1630$–$1480\ cm^{-1}$and $\nu_5(B_2) \approx 1300$–$1160\ cm^{-1}$] and a strong band at $1384\ cm^{-1}$ for the NO_3^- counterion are also observed.[24] In the spectra of **2a**, and in the same region, the strong intensity band at $1384\ cm^{-1}$ is attributed to the presence of ionic nitrates. In the spectra of **2b**, the corresponding band appears at $1383\ cm^{-1}$. A very important feature for the characterization of **2a** and **2b** is the presence of a strong band at ca. $880\ cm^{-1}$, not observed in the spectra of **1**, **3** and free tptz, which is characteristic of the asymmetric stretching vibration of the Fe^{III}–O–Fe^{III} moiety, ν_{as}(Fe–O–Fe).[25] The Mössbauer data (vide infra) are also indicative of the presence of an oxido-bridged diferric moiety in **2**. In the spectra of **3**, apart from the strong broad band at ca. $1100\ cm^{-1}$ attributed to the perchlorate counterions, notable are the weak bands in the region 3230–$3100\ cm^{-1}$, which may be assigned to the ν(NH) stretching vibration of the crystallographically established $tptzH^+$ ligand.[26] The shifting of these bands to lower frequencies is consistent with the hydrogen-bonding interactions through the NH group of the $tptzH^+$ ligand, which is established by the crystallographic data. These bands are not observed in the spectra of **1**, in agreement with the crystallographically established presence of neutral tptz, whereas their appearance in the spectra of **2a** and **2b** may be considered as evidence for the presence of $tptzH^+$ in both compounds.

Description of the Structures

The molecular structure of complex **1** is shown in Figure 1 and selected bond lengths and angles are listed in Table 1. The structure of **1** consists of the cationic complex $[Fe(tptz)(NO_3)(MeOH)_2]^+$ and a nitrate counterion. The coordination geometry around the Fe^{II} ion is pentagonal bipyramidal and comprises three nitrogen atoms of the tptz ligand and four oxygen atoms belonging to a chelating NO_3^- anion and two methanol molecules. The equatorial positions of the pentagonal bipyramid are occupied by the nitrogen atoms of the tptz and the chelating nitrato ligand, and the apical positions are occupied by the two coordinated methanol molecules. The tptz acts as a tridentate ligand and is coordinated through one triazine nitrogen atom and the two adjacent pyridine nitrogen atoms, adopting the terpy-like coordination mode (**I** in Scheme 1). The N_3O_2 atom-set in the equatorial plane and Fe^{II} are coplanar, and the largest deviation is 0.07 Å for O2. The same feature is observed in the cationic complex $[Fe(dapsc)(H_2O)Cl]^+$ [dapsc = 2,6-diacetylpyridine bis(semicarbazone)] in which the N_3O_2 atom-set belongs to the dapsc ligand,[27] unlike the case of the cationic complex $[Fe(N_5)(H_2O)_2]^{2+}$ (N_5 = a pentadentate macrocyclic ligand) where the FeN_5 atoms in the equatorial plane are not coplanar.[28] The Fe–$O_{methanol}$ bond lengths in the apical positions of the pentagonal bipyramid are ca. 2.13 Å and are very similar to that found in $[Fe(dapsc)(H_2O)Cl]^+$ (2.15 Å) and substantially shorter than that in $[Fe(N_5)(H_2O)_2]^{2+}$ (2.22 Å). On the other hand, the Fe–$N_{pyridine}$ bond lengths are ca. 2.29 Å and are longer than that found in $[Fe(N_5)(H_2O)_2]^{2+}$ (2.22 Å) and substantially longer than the Fe–$N_{triazine}$ bond length of 2.14 Å. The nitrate anion is asymmetrically coordinated to the Fe^{II} ion [Fe–O1 = 2.335(4) and Fe–O2 = 2.201(4) Å]. To the best of our knowledge, there is no other example of heptacoordinate Fe^{II}–nitrato complex; only two examples of hexacoordinate Fe^{II}–nitrato complexes have been structurally characterized.[14,15] In the case of the heptacoordinate manganese(II) complex,[29] $[Mn^{II}L_3(NO_3)_2]$ (L = dimethylurea), the chelating nitrato anions occupy the equatorial positions of the pentagonal bipyramid around Mn^{II}; one of the nitrato ligands is symmetrically coordinated (Mn–O ca. 2.37 Å) and the other one is asymmetrically coordinated to Mn^{II} (Mn–O = 2.33 and 2.38 Å). The structural features of **1** are analogous to those observed for the recently reported Mn^{II} complex $[Mn(tptz)(NO_3)(H_2O)_2](NO_3)$.[30]

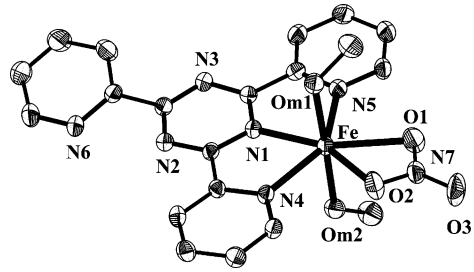

Figure 1. Partially labelled ORTEP plot of the cation of **1** with ellipsoids drawn at the 30% probability level. Hydrogen atoms have been omitted for clarity.

Table 1. Selected bond lengths [Å] and angles [°] for complex **1**.

Distances			
Fe–Om1	2.135(3)	Fe–N4	2.285(3)
Fe–N1	2.146(3)	Fe–N5	2.299(4)
Fe–Om2	2.142(3)	Fe–O1	2.335(4)
Fe–O2	2.201(4)		
Angles			
Om1-Fe–N1	88.6(1)	N1–Fe–N5	71.7(1)
Om1–Fe–Om2	178.6(1)	Om2–Fe–N5	91.3(1)
N1–Fe–Om2	90.1(1)	O2–Fe–N5	135.5(1)
Om1–Fe–O2	92.2(1)	N4–Fe–N5	143.8(1)
N1–Fe–O2	152.8(1)	Om1–Fe–O1	94.4(1)
Om2–Fe–O2	88.8(1)	N1–Fe–O1	151.8(1)
Om1–Fe–N4	92.7(1)	Om2–Fe–O1	87.1(1)
N1–Fe–N4	72.1(1)	O2–Fe–O1	55.2(1)
Om2–Fe–N4	86.3(1)	N4–Fe–O1	135.5(1)
O2–Fe–N4	80.7(1)	N5–Fe–O1	80.3(1)
Om1–Fe–N5	88.8(1)		

The central triazine ring and the two coordinated adjacent pyridine rings of the tptz are coplanar (largest deviation 0.05 Å for C11), while the uncoordinated pyridine ring is twisted 16.3° around the C3–C14 bond with respect to the triazine ring.

The nitrate counteranion is hydrogen bonded to one of the coordinated methanol molecules [HOm1···O4 (x, y, z) = 1.922 Å, Om1···O4 = 2.797 Å, Om1-HOm1···O4 = 170.7°], while the second coordinated methanol is hydrogen bonded to the uncoordinated pyridine nitrogen of a centrosymmetrically related cation of **1**, which leads to the formation of dimers [HOm2···N6 (-x, –y, –z) = 2.098 Å, Om2···N6 = 2.754 Å, Om2-HOm2···N6 = 142.7°] (Figure 2). The dimers are further stabilized by π–π stacking interactions between the aromatic rings of the tptz molecules. The distance between the centroids of the two rings is 3.663(2) Å. The closest Fe···Fe distance in the dimer is 7.89 Å.

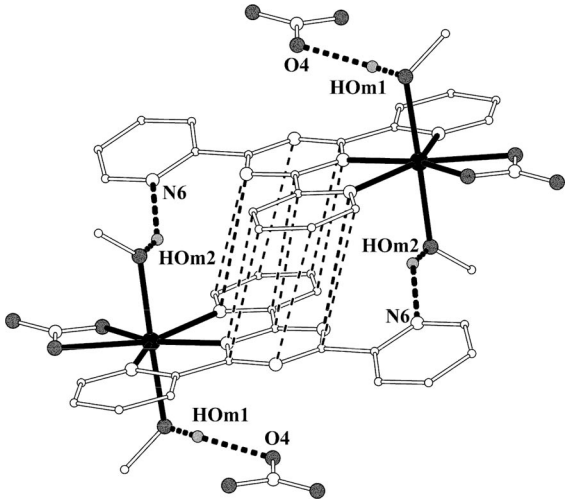

Figure 2. Partially labeled ORTEP plot of the dimers formed in the crystal structure of **1** as a result of hydrogen-bonding interactions (bold dashed lines) and π–π stacking interactions (thin dashed lines). (Fe: black, O: dark grey, N: open large circles, C: open small circles, H: light grey).

The molecular structure of **3** is given in Figure 3, and selected bond lengths and angles are listed in Table 2. The structure of **3** consists of the cationic complex $[Fe(tptzH)_2]^{4+}$ and four perchlorate anions. The coordination geometry around the Fe^{II} ion is a distorted octahedral, comprising triazine nitrogen atoms of each tptz in the apical positions and four pyridine nitrogen atoms from the two tptz ligands that define the equatorial plane. Thus, each tptz ligand adopts a terpy-like coordination mode (**I** in Scheme 1). The Fe–$N_{triazine}$ and the Fe–$N_{pyridine}$ bond lengths of ca. 1.85 and ca. 2.00 Å, respectively, are comparable to the Fe–N bond lengths found in low-spin (at room temperature) octahedral complexes $[Fe^{II}(phen)_3](C_5H_4COR)_2$ (R = Me, Ph)[31] and $[Fe^{II}(C16\text{-terpy})_2](ClO_4)_2$ (where C16-terpy = 4′-hexadecyloxy-2,2′:6′,2′′-terpyridine)[32] as well as in $[Fe^{II}L_2](PF_6)_2$ [L = 4′-(4,7,10-trioxadec-1-yn-10-yl)-2,2′:6′;2′′-terpyridine][33] and $[Fe^{II}(tppz)_2][Fe^{II}(NCS)_4]$ [tppz = 2,3,5,6-tetrakis(2-pyridyl)-pyrazine],[34] which all present N_6 coordination environments. In the case of high-spin (at room temperature) octahedral complexes $[Fe^{II}(phen)_2(NCS)_2]$[35] and $[Fe^{II}(2,9\text{-dmp})_2(NCS)_2]$ (2,9-dmp = 2,9-dimethyl-1,10-phenanthroline),[36] which also present N_6 coordination environments, the corresponding Fe–N bond lengths are substantially longer (ca. 2.27 and ca. 2.20 Å, respectively). The low-spin state of **3** has been confirmed by Mössbauer spectroscopy (vide infra).

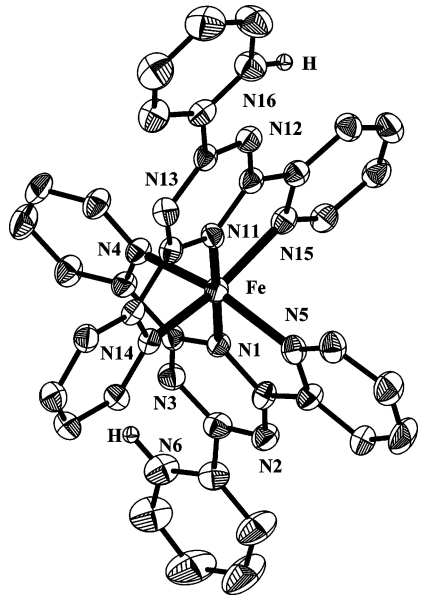

Figure 3. Partially labelled ORTEP plot of the cation of **3** with ellipsoids drawn at the 30% probability level. Hydrogen atoms on the pyridine nitrogen atoms are shown, the rest have been omitted for clarity.

Table 2. Selected bond lengths [Å] and angles [°] for complex **3**.

Distances			
Fe–N1	1.854(5)	Fe–N5	1.999(6)
Fe–N11	1.859(5)	Fe–N15	1.999(6)
Fe–N14	1.992(6)	Fe–N4	2.008(6)
Angles			
N1–Fe–N11	178.9(2)	N14–Fe–N15	160.7(2)
N1–Fe–N14	99.0(2)	N5–Fe–N15	87.4(2)
N11–Fe–N14	80.0(2)	N1–Fe–N4	80.3(2)
N1–Fe–N5	80.1(2)	N11–Fe–N4	99.3(2)
N11–Fe–N5	100.2(2)	N14–Fe–N4	87.5(2)
N14–Fe–N5	94.7(2)	N5–Fe–N4	160.4(2)
N1–Fe–N15	100.3(2)	N15–Fe–N4	96.9(2)
N11–Fe–N15	80.7(2)		

The central triazine ring and the two adjacent pyridine rings of each tptz ligand coordinated to Fe^{II} are coplanar and almost perpendicular to each other and form an angle of 81.2°. The protonated uncoordinated pyridine ring of each tptz ligand is twisted by 10.3° and 11.8° with respect to the triazine ring around the C2–C14 and C22–C34 bonds, respectively. Complex **3** is the first compound containing two $tptzH^+$ cations as ligands. As far as we know, there are two Ni^{II} complexes, $[Ni(tptzH)(H_2O)_3]X_3$ (X = Br^-, NO_3^-),[37] containing $tptzH^+$ in which the protonated pyridine ring is less twisted with respect to the triazine ring (ca. 4–5°). On the other hand, in complexes containing two neutral tptz molecules, such as $[Zn(tptz)_2]^{2+}$,[38] $[Co(tptz)_2]^{2+}$[39] and $[Ru(tptz)_2]^{2+}$,[2c] the twisting angle ranges from ca. 4.5 to 20°.

The protonated nitrogen atom of the third pyridine group of each tptz participates in hydrogen-bonding interactions with the perchlorate anions [HN6···O5 (x, 0.5 – y, –0.5 + z), 1.888 Å; N6···O5, 2.784 Å; N6–HN6···O5, 164.6°; HN16···O9 (–0.5 + x, 0.5 – y, 1 – z), 1.875 Å; N16···O9, 2.801 Å; N16–HN16···O9 158.0°].

Compounds **1** and **3** join a small family of crystallographically characterized iron complexes of tptz; the other complexes are $[Fe^{III}Cl_3(tptz)]\cdot MeCN$,[2a] $[Fe^{II}(tptz)_2]Cl_2\cdot 4H_2O$,[40] $[Fe^{III}_2OCl_4(tptz)_2]\cdot 2H_2O$[40] and $[Fe^{III}_2O(tptz)_2\{N(CN)_2\}_2](NO_3)_2$.[41]

Mössbauer Spectroscopy

Zero-field Mössbauer spectrum of a sample that contains microcrystals of **1** was recorded in the 4.2–293 K temperature range and presents a quadrupole-split doublet. The spectrum recorded at 78 K is shown in Figure 4. At this temperature, the isomer shift is δ = 1.27(1) mm s^{-1} and the quadrupole splitting is ΔE_Q = 3.38(1) mm s^{-1}. These parameters are typical for high-spin ferrous ions with N/O ligands. The high-spin ferrous character of the complex is retained in the whole temperature range, with a decrease in the value for the isomer shift because of the second-order Doppler effect for $T > 78$ K.[42]

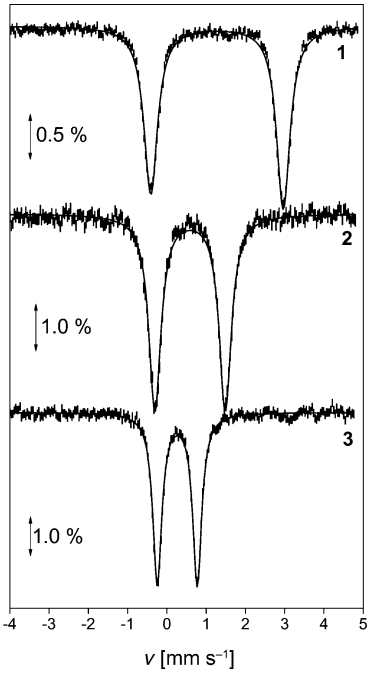

Figure 4. Mössbauer spectra from powder samples of complexes **1**, **2** and **3** at 78 K.

In Figure 5, the temperature dependence of ΔE_Q is shown. The low temperature value of ca. 3.4 mm s^{-1} suggests that the ground state is an orbital singlet. Above 78 K, ΔE_Q decreases, which indicates the presence of low-lying orbital states. The temperature dependence of ΔE_Q may be used to estimate the separation of these excited states from the ground state. We consider a ^{5}D ion in an octahedral field for which axial and rhombic distortions totally lift the orbital degeneracy of the ground T_{2g} state. Within this picture, the two excited orbitals are located at a distance of Δ_1 and Δ_2 from the ground state. As an approximation, the temperature dependence of ΔE_Q is modelled with Equation (1).[43]

$$\Delta E_Q = \Delta E_Q(0)\times\frac{1+e^{-\frac{2\Delta_1}{kT}}+e^{-\frac{2\Delta_2}{kT}}-e^{-\frac{\Delta_1}{kT}}-e^{-\frac{\Delta_2}{kT}}-e^{-\frac{(\Delta_1+\Delta_2)}{kT}}}{1+e^{-\frac{\Delta_1}{kT}}+e^{-\frac{\Delta_2}{kT}}} \quad (1)$$

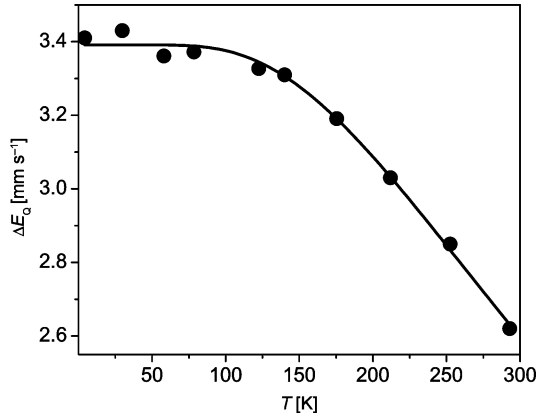

Figure 5. Temperature dependence of ΔE_Q for complex **1**. Solid line is the theoretical curve obtained as explained in the text.

Fitting of the experimental data with this model yields $\Delta E_Q(0) = 3.39 \pm 0.01$ mm s^{-1}, $\Delta_1 = 400 \pm 20$ cm^{-1}, and $\Delta_2 = 650 \pm 80$ cm^{-1}.

The Mössbauer spectrum from powdered samples of **2b** presents one quadrupole-split doublet in the 4.2–300 K temperature range. At 78 K, the isomer shift is δ = 0.59(1) mm s^{-1} and the quadrupole splitting is ΔE_Q = 1.79(2) mm s^{-1} (Figure 4). At room temperature, δ decreases as a result of the second-order Doppler effect.[42] The isomer shift is consistent with a high-spin ferric ion in an octahedral environment comprising N/O ligands. The room temperature Mössbauer spectrum from a powdered sample of **2a** is almost identical to that of **2b**, which indicates that **2a** and **2b** are similar compounds. The quadrupole splitting is rather large for a high-spin ferric ion. Exceptionally large ΔE_Q values (>3.00 mm s^{-1}) have been reported for mononuclear high-spin ferric complexes in which the coordination of the iron adopts a trigonal-planar geometry.[44] Such complexes are extremely rare and it is considered highly unlikely that complex **2** belongs to this category. On the other hand, quadrupole splittings in the range 1.00–2.00 mm s^{-1} have been reported for Fe^{III}–O–Fe^{III} dimers.[45] The crystal structure of the oxido-bridged diferric complex $[Fe_2O(tptz)_2\{N(CN)_2\}_2](NO_3)_2$ was reported recently;[41] this compound exhibits a quadrupole splitting consistent with that for a Fe^{III}–O–Fe^{III} dimer.[46] On the basis of the Mössbauer parameters and in particular on the value of ΔE_Q, the oxido-bridged diferric complex $[Fe(tptz)Cl_2]_2O\cdot 2H_2O$ was proposed to be formed after the high-spin ferrous compound $[Fe(tptz)Cl_2]$ was exposed to air.[47] We therefore suggest

that **2** is an oxido-bridged diferric complex, in agreement with infrared spectroscopic features and elemental analyses.

The Mössbauer spectrum from a powder sample of **3** presents a quadrupole-split doublet with parameters δ = 0.26(1) mm s^{-1} and ΔE_Q = 1.01(2) mm s^{-1} at 78 K and δ = 0.19(1) mm s^{-1} and ΔE_Q = 1.00(2) mm s^{-1} at 293 K. These parameters are consistent with a low-spin ferrous ion in the whole temperature range.[42] Apparently, ligation of two tptz moieties to the iron site results in a stronger crystal field, which favours a low-spin configuration. Moreover, the rather large ΔE_Q value is consistent with a distorted octahedral environment around the iron ion.

Magnetic Susceptibility Measurements

The $\chi_M T$ value for **1** at 300 K is 2.90 cm^3 mol^{-1} K, which is slightly below the spin-only value of an isolated S = 2 ion (3.00 cm^3 mol^{-1} K). The $\chi_M T$ product decreases very slowly down to ca. 40 K and then drops rapidly down to 1.36 cm^3 mol^{-1} K at 2.2 K (Figure 6). This behaviour is attributed to the Zeeman and zero-field splitting effects of the Fe^{II} ions.

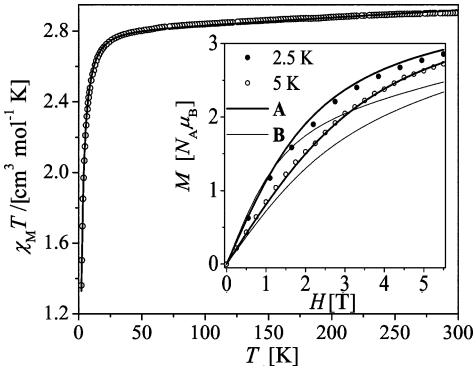

Figure 6. $\chi_M T$ vs. T data for **1** and the best fit (solution **A**, $D > 0$) according to the model mentioned in the text. M vs. H simulations corroborate solution **A** as the best.

To fit the experimental data, an isolated S = 2 ion was considered, which exhibits a single-ion axial anisotropy D, according to the Hamiltonian of Equation (2).

$$\hat{H} = D\hat{S}_z^2 + \mu_B \mathrm{H}\tilde{\mathrm{g}}\hat{\mathrm{S}} \quad (2)$$

Two solutions were obtained when the data were fitted, one for $D > 0$ (**A**) and one for $D < 0$ (**B**), with best-fit parameters, D = +5.5 cm^{-1}, g = 1.93, TIP (temperature-independent paramagnetism) = 417×10^{-6} cm^3 mol^{-1} and R = 1.7×10^{-5} (**A**), and D = –5.4 cm^{-1}, g = 1.93, TIP = 361×10^{-6} cm^3 mol^{-1} and R = 1.0×10^{-4} (**B**). Clearly, solution **A** ($D > 0$) is of superior quality. However, since the estimation of the sign of D is not straightforward from magnetic susceptibility data alone, magnetization isotherms were recorded at 2.5 and 5 K. The magnetization M vs. applied magnetic field H curves were calculated from the parameters of each solution and compared to the experimental M vs. H data. Solution **A**, once again, reproduced the experimental data in a much more satisfactory manner (inset in Figure 6).

Magnetic susceptibility measurements on **2** were carried out on powdered samples. These were performed to better establish its formulation as "[Fe^{III}_2O(tptzH)$_2$(H$_2$O)$_4$](NO$_3$)$_6$·2H$_2$O", which was derived from microanalytical and spectroscopic (IR, Mössbauer) data. The molecular weight for **2** was based on that formulation and calculated by including the water solvates. However, disregarding the solvates did not significantly alter the magnetic data and the resulting fits. The $\chi_M T$ value of **2** at 300 K is 0.78 cm^3 mol^{-1} K (Figure 7), lower than the theoretically expected value for two noninteracting S = 5/2 spins (8.75 cm^3 mol^{-1} K), which suggests strong antiferromagnetic interactions. This is corroborated by the decrease in $\chi_M T$ upon cooling. The value drops to a plateau of 0.083 cm^3 mol^{-1} K below 50 K, which is indicative of a paramagnetic impurity fraction, ρ.

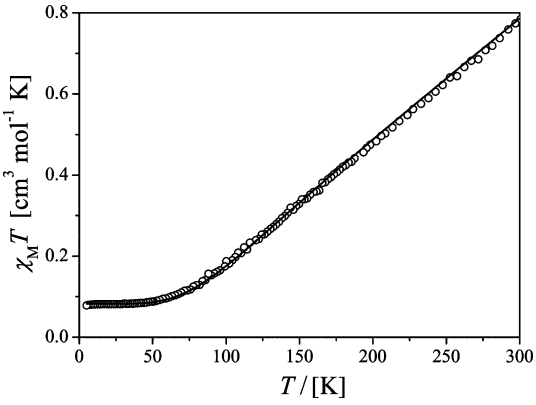

Figure 7. $\chi_M T$ vs. T data for **2** and the best fit according to the model mentioned in the text.

A simple model of two interacting S = 5/2 spins was used for the interpretation of the magnetic susceptibility data, with the respective spin Hamiltonian [Equation (3)].

$$\hat{H} = -2J\hat{S}_1\hat{S}_1 \quad (3)$$

Fits to the data yielded parameters J = –117 cm^{-1}, g = 2 (fixed) and ρ = 2% (R = 4.9×10^{-4}). These values are typical for oxido-bridged diferric complexes, and thus lend further support to our previous conclusions.

Conclusions

Compound [Fe^{II}(tptz)(NO$_3$)(MeOH)$_2$](NO$_3$) (**1**), representing the first example of a structurally characterized heptacoordinate high-spin Fe^{II}–nitrato complex, has been isolated from the 1:1:2 Fe(NO$_3$)$_3$·9H$_2$O/tptz/Ph$_2$C(OH)CO$_2$H reaction in MeOH, as a result of aerobic reduction of Fe^{III} to Fe^{II}. The same reaction also afforded a ferric complex that was formulated as [Fe^{III}_2O(tptzH)$_2$(H$_2$O)$_4$](NO$_3$)$_6$·2H$_2$O (**2**) by microanalytical, spectroscopic (IR, Mössbauer) and magnetic susceptibility data. Replacement of the oxidative NO_3^- ions in the above reaction with ClO_4^- resulted in the quantitative reduction of the Fe^{III} ions to yield

exclusively the low-spin hexacoordinate complex $[Fe^{II}(tptzH)_2](ClO_4)_4$ (**3**) from MeOH or MeCN solutions. The above reaction mixtures constitute quite complicated systems in terms of equilibria and/or kinetics, in which the exact reducing agents cannot yet be determined. We assume that the presence of both benzilic acid and tptz in the reaction mixtures is determinative for the aerobic Fe^{III} to Fe^{II} reduction and for the stabilization of the ferrous complexes **1** and **3**.

Experimental Section

General Procedures and Materials: All manipulations were performed under aerobic conditions by using materials as received (Aldrich Co). All chemicals and solvents were of reagent grade. Elemental analysis for carbon, hydrogen, and nitrogen was performed on a Perkin–Elmer 2400/II automatic analyzer. Infrared spectra were recorded as KBr pellets in the range 4000–500 cm^{-1} on a Bruker Equinox 55/S FTIR spectrophotometer. Mössbauer spectra were recorded with a constant acceleration spectrometer using a ^{57}Co (Rh) source at room temperature and a variable-temperature Oxford cryostat. Variable-temperature magnetic susceptibility measurements were carried out on a polycrystalline sample of **1** in the 2–300 K temperature range and on a powdered microcrystalline sample of **2** in the 5–300 K temperature range by using a Quantum Design MPMS SQUID susceptometer under magnetic fields of 1 T for **1** and 0.2 T for **2**. Magnetization isotherms between 0 and 5.4 T for **1** were collected at 2 and 5 K. Diamagnetic corrections for the complexes were estimated from Pascal's constants. Data were corrected with the standard procedure for the contribution of the sample holder and diamagnetism of the sample. The magnetic susceptibility was computed by exact calculation of the energy levels associated with the spin Hamiltonian through diagonalization of the full-matrix with a general program for axial symmetry.[48] Least-squares fittings were accomplished with an adapted version of the function-minimization program MINUIT.[49] The error-factor R is defined as $R = \Sigma[(\chi_{exp} - \chi_{calcd.})^2]\cdot(N\chi^2_{exp})^{-1}$, where N is the number of experimental points. Simulations of the magnetization M vs. applied field H were carried out with the MAGPACK program package, by using parameters derived from fits of the magnetic susceptibility.[50]

Preparation of 1 and 2a: Solid benzilic acid (0.228 g, 1.00 mmol) was added to a stirred orange solution of $Fe(NO_3)_3\cdot 9H_2O$ (0.202 g, 0.50 mmol) in MeOH (20 mL). The colour of the solution immediately changed to red, and after 5 min of stirring, solid tptz (0.156 g, 0.50 mmol) was added. The colour of the solution immediately turned to deep purple and the stirring was continued for 30 min. By that time, an orange precipitate (**2a**) formed, which was filtered off and dried in vacuo. Vapour diffusion of Et_2O to the deep purple filtrate afforded blue needlelike crystals of $[Fe^{II}(tptz)(NO_3)(MeOH)_2](NO_3)$ (**1**), followed by gradual decolourization of the original deep purple filtrate to yellow. (Yield: 0.052 g, ca. 19%). The crystals of **1** were collected by filtration and dried in vacuo. $C_{20}H_{20}FeN_8O_8$ (556.29): calcd. C 43.18, H 3.62, N 20.14; found C 43.16, H 3.61, N 20.12. FTIR (KBr pellets): $\tilde{\nu}$ = 3423 (br.), 3063 (w), 1637 (w), 1574 (m), 1556 (s), 1530 (s), 1489 (s), 1480 (sh.), 1439 (m), 1384 (vs), 1313 (m), 1293 (s), 1258 (m), 1183 (w), 1164 (w), 1096 (w), 1050 (m), 1009 (s), 859 (w), 825 (w), 814 (w), 771 (s), 677 (w), 666 (m), 633 (m), 490 (w), 417 (w) cm^{-1}.

The orange precipitate was formulated as "$[Fe^{III}_2O(tptzH)_2(H_2O)_4](NO_3)_6\cdot 2H_2O$" (**2a**) by elemental analysis and IR and Mössbauer spectroscopy. $C_{36}H_{38}Fe_2N_{18}O_{25}$ (1234.50): calcd. C 35.02, H 3.10, N 20.42; found C 34.92, H 3.12, N 20.32. FTIR (KBr pellets): $\tilde{\nu}$ = 3425 (br.), 3238 (vw), 3161 (vw), 3103 (sh.), 3068 (m), 1615 (m), 1575 (s), 1560 (vs), 1544 (vs), 1490 (s), 1422 (sh.), 1397 (sh.), 1384 (vs), 1362 (sh.), 1328 (sh.), 1308 (m), 1292 (s), 1229 (m), 1178 (w), 1161 (w), 1114 (w), 1093 (m), 1054 (m), 1037 (m), 1012 (s), 880 (s), 861 (s), 834 (w), 804 (w), 776 (vs), 752 (w), 675 (s), 666 (m), 637 (m), 616 (m), 479 (w), 440 (w), 422 (w) cm^{-1}. Yield: 0.189 g, ca. 31%.

Preparation of 2b: Solid tptz (0.312 g, 1.00 mmol) was added to a stirred orange solution of $Fe(NO_3)_3\cdot 9H_2O$ (0.404 g, 1.00 mmol) in MeOH (20 mL). The colour of the solution immediately turned to red, and the stirring was continued for 30 min. By that time, the solution was blue and an orange precipitate (**2b**) had formed, which was filtered off and dried in vacuo. Microanalytical and spectroscopic (IR, Mössbauer) data were identical to those of the orange precipitate derived during the preparation of **1**. (Yield: 0.49 g, 79%). Vapour diffusion of Et_2O into the blue filtrate yielded an orange precipitate, followed by decolourization of the solution after 3 d.

In an attempt to isolate X-ray quality crystals of **2**, solid tptz (0.078 g, 0.25 mmol) was placed on a paper cone and allowed to slowly dissolve in an orange solution of $Fe(NO_3)_3\cdot 9H_2O$ (0.101 g, 0.25 mmol) in MeOH (20 mL), which was previously placed in a test tube. The tube was sealed and after 3 d, the colour of the solution was greenish-red, and small portions of orange–red microcrystalline material along with large amounts of orange powder were precipitated. Solutions of variable concentrations were tested in order to isolate X-ray quality crystals of **2**, but in every case they afforded microcrystalline products.

Preparation of 3: Method A. Solid benzilic acid (0.228 g, 1.00 mmol) was added to a stirred orange solution of $Fe(ClO_4)_3\cdot 9H_2O$ (0.258 g, 0.50 mmol) in MeCN (20 mL). The colour of the solution immediately changed to red, and after 5 min of stirring, solid tptz (0.156 g, 0.50 mmol) was added. The colour of the solution immediately turned to yellowish brown. The reaction mixture was heated at reflux for 10 min to give a deep-blue solution and a small amount of a blue precipitate, which was filtered off. The deep blue filtrate was left so that slow evaporation can take place. After 2 d, X-ray quality blue crystals of **3** formed, which were collected by filtration and dried in vacuo. (Yield: 0.43 g, ca. 80%). $C_{36}H_{26}Cl_4FeN_{12}O_{16}$ (1080.34): calcd. C 40.02, H 2.43, N 15.56; found C 39.87, H 2.44, N 15.49. FTIR (KBr pellets): $\tilde{\nu}$ = 3436 (br.), 3233 (w), 3159 (w), 3102 (w), 3072 (w), 1614 (s), 1573 (s), 1557 (w), 1538 (m), 1509 (vs), 1476 (w), 1458 (w), 1452 (sh.), 1418 (s), 1359 (s), 1308 (m), 1288 (m), 1268 (m), 1241 (m), 1182 (w), 1101 (vs), 1085 (vs), 1042 (s), 1014 (m), 932 (w), 772 (sh.), 764 (s), 750 (m), 660 (m), 621 (s), 514 (w), 494 (w), 464 (w), 446 (w) cm^{-1}. Method B. The same reaction as above (Method A) was carried out in MeOH (20 mL). After heating at reflux for 30 min, a deep-blue precipitate formed, which was filtered off and dried in vacuo. Microanalytical and spectroscopic (IR, Mössbauer) data were identical to those of **3**.

X-ray Crystallography: A blue needlelike crystal of **1** ($0.10 \times 0.18 \times 0.85$ mm) was mounted in a capillary, and a blue prismatic crystal of **3** ($0.20 \times 0.65 \times 0.65$ mm) was mounted in air and covered with epoxy glue. Diffraction measurements were made on a Crystal Logic Dual Goniometer diffractometer with graphite monochromated Mo radiation. Important crystal data and parameters for data collection are reported in Table 3. Unit cell dimensions were determined and refined by using the angular settings of 25 automatically centred reflections in the range $11° < 2\theta < 23°$.

Three standard reflections monitored every 97 reflections showed less than 3% intensity fluctuation and no decay. Lorentz, polarization and ψ-scan absorption corrections (for **3** only) were applied by using Crystal Logic software. The structures were solved by direct methods with SHELXS-97[51] and refined by full-matrix least-squares techniques on F^2 with SHELXL-97.[52] Further experimental crystallographic details for **1**: $2\theta_{max} = 48°$, scan speed 1.5°/min; scan range 1.6 +$\alpha_1\alpha_2$ separation; reflections collected/unique/used, 4025/3717 [$R_{int} = 0.0205$]/3717; 392 parameters refined; $(\Delta/\sigma)_{max} = 0.002$; $(\Delta\rho)_{max}/(\Delta\rho)_{min} = 0.359/-0.242$ e/Å^3; R/R_w (for all data), 0.0807/0.1184. Hydrogen atoms (except those of the methyl groups, which were introduced at calculated positions as riding on bonded atoms) were located by difference maps and were refined isotropically. All non-H atoms were refined anisotropically. Further experimental crystallographic details for **3**: $2\theta_{max} = 50°$, scan speed 6.0°/min; scan range 1.6 +$\alpha_1\alpha_2$ separation; reflections collected/unique/used, 6186/6186 [$R_{int} = 0.0000$]/6186; 744 parameters refined; $(\Delta/\sigma)_{max} = 0.011$; $(\Delta\rho)_{max}/(\Delta\rho)_{min} = 0.604/-0.469$ e/Å^3; R/R_w (for all data), 0.1209/0.2178. Hydrogen atoms on aromatic carbon atoms were introduced at calculated positions as riding on bonded atoms; those of the pyridine nitrogen atoms were located by difference maps and were refined isotropically. All non-H atoms were refined anisotropically. The oxygen atoms of three of the perchlorate anions were found disordered and were refined anisotropically over two positions with occupation factors summing one. CCDC-687268 (for **1**) and CCDC-687269 (for **3**) contain the supplementary crystallographic data for this paper. These data can be obtained free of charge from The Cambridge Crystallographic Data Centre via www.ccdc.cam.ac.uk/data_request/cif.

Table 3. Crystallographic data for complexes **1** and **3**.

	1	**3**
Formula	$C_{20}H_{20}FeN_8O_8$	$C_{36}H_{26}Cl_4FeN_{12}O_{16}$
F_w	556.29	1080.34
Space group	$P2_1/c$	$Pbca$
T [°C]	25	25
λ [Å]	0.71073 (Mo-K_α)	0.71073 (Mo-K_α)
a [Å]	7.572(6)	23.09(1)
b [Å]	24.33(2)	14.557(7)
c [Å]	13.029(9)	25.90(1)
β [°]	98.80(2)	
V [Å^3]	2371(3)	8706(7)
Z	4	8
$\rho_{calcd.}$ [g cm^{-3}]	1.558	1.649
μ (Mo-K_a) [mm^{-1}]	0.70	0.679
R_1[a]	0.0477[b]	0.0667[c]
wR_2[a]	0.1040[b]	0.1520[c]

[a] $w = 1/[\sigma^2(F_o^2) + (aP)^2 + bP]$ and $P = [(\max\{F_o^2,0\}) + 2F_c^2]/3$; $R_1 = \Sigma(|F_o| - |F_c|)/\Sigma(|F_o|)$ and $wR_2 = \{\Sigma[w(F_o^2 - F_c^2)^2]/\Sigma[w(F_o^2)^2]\}^{1/2}$. [b] for 2672 reflections with $I > 2\sigma(I)$. [c] For 4180 reflections with $I > 2\sigma(I)$.

Supporting Information (see footnote on the first page of this article): Mössbauer spectra of **3** (prepared by Method B, see Experimental Section) and of the orange precipitate for which an oxido-bridged diferric structure is proposed.

[1] a) N. Gupta, N. Grover, G. A. Neyhart, P. Singh, H. H. Thorp, *Inorg. Chem.* **1993**, *32*, 310–316; b) M. Maekawa, T. Minematsu, H. Konaka, K. Sugimoto, T. Kuroda-Sowa, Y. Suenaga, M. Munakata, *Inorg. Chim. Acta* **2004**, *357*, 3456–3472.

[2] a) S. A. Cotton, V. Franckevicius, J. Fawcett, *Polyhedron* **2002**, *21*, 2055–2061; b) P. Paul, B. Tyagi, A. K. Bilakhiya, M. M. Bhadbhade, E. Suresh, G. Ramachandraiah, *Inorg. Chem.* **1998**, *37*, 5733–5742; c) P. Paul, B. Tyagi, M. M. Bhadbhade, E. Suresh, *J. Chem. Soc., Dalton Trans.* **1997**, 2273–2277; d) A. Majumder, G. Pilet, M. T. Garland Rodriguez, S. Mitra, *Polyhedron* **2006**, *25*, 2550–2558; e) A. Das, G. M. Rosair, M. S. El Fallah, J. Ribas, S. Mitra, *Inorg. Chem.* **2006**, *45*, 3301–3306.

[3] a) W. A. Embry, G. H. Ayres, *Anal. Chem.* **1968**, *40*, 1499–1501; b) M. J. Janmohamed, G. H. Ayres, *Anal. Chem.* **1972**, *44*, 2263–2268.

[4] a) R. Wietzke, M. Mazzanti, J.-M. Latour, J. Pécaut, *Inorg. Chem.* **1999**, *38*, 3581–3585; b) I. Hagstrom, L. Spjuth, A. Enarsson, J. O. Liljenzin, M. Skalberg, M. J. Hudson, P. B. Iveson, C. Madic, P.-Y. Cordier, C. Hill, N. François, *Solvent Extr. Ion Exch.* **1999**, *17*, 221–242; c) P. Vitorge, *Complexation de lanthanides et d'actinides trivalents par la TPTZ. Application en extraction liquide-liquide.* **1985**, Report **1984**, CEA–R–5270; d) D. A. Durham, G. H. Frost, F. A. Hart, *J. Inorg. Nucl. Chem.* **1969**, *31*, 571–574; e) E. Bou-Maroun, A. Boos, G. J. Goetz-Grandmont, *Sep. Purif. Techn.* **2007**, *53*, 250–258; f) E. Bou-Maroun, G. J. Goetz-Grandmont, A. Boos, *Sep. Sci. Techn.* **2007**, *42*, 1913–1930.

[5] a) F. P. Pruchnik, P. Jakimowicz, Z. Ciunik, J. Zakrzewska-Czerwinska, A. Opolski, E. Wojdat, *Inorg. Chim. Acta* **2002**, *334*, 59–66; b) J. P. H. Charmant, A. H. M. M. Jahan, N. C. Norman, A. G. Orpen, T. J. Podesta, *CrystEngComm* **2004**, *6*, 29–33; c) M. A. Harvey, S. Baggio, R. Baggio, *Acta Crystallogr., Sect. C* **2004**, *60*, m498-m500; d) M. Harvey, S. Baggio, S. Russi, R. Baggio, *Acta Crystallogr., Sect. C* **2003**, *59*, m171-m174; e) J. M. Harrowfield, H. Miyamae, B. W. Skelton, A. A. Soudi, A. H. White, *Aust. J. Chem.* **1996**, *49*, 1157–1164.

[6] a) E. Freire, S. Baggio, J. C. Munoz, R. Baggio, *Acta Crystallogr., Sect. C* **2002**, *58*, m221-m224; b) K. M. Lo, V. G. K. Das, S. W. Ng, *Acta Crystallogr., Sect. C* **1999**, *55*, 1058–1061; c) S. A. Cotton, V. Franckevicius, M. F. Mahon, L. L. Ooi, P. R. Raithby, S. J. Teat, *Polyhedron* **2006**, *25*, 1057–1068; d) S. Sharma, M. Chandra, D. S. Pandey, *Eur. J. Inorg. Chem.* **2004**, 3555–3563.

[7] X. Chen, F. J. Femia, J. W. Babich, J. A. Zubieta, *Inorg. Chem.* **2001**, *40*, 2769–2777.

[8] M. Chandra, A. N. Sahay, D. S. Pandey, M. C. Puerta, P. Valerga, *J. Organomet. Chem.* **2002**, *648*, 39–48.

[9] L. Zhang, X.-Q. Lu, Q. Zhang, C.-L. Chen, B.-S. Kang, *Transition Met. Chem.* **2005**, *30*, 76–81.

[10] J. Halfpenny, R. W. H. Small, *Acta Crystallogr., Sect. B* **1982**, *38*, 939–942.

[11] T. Glaser, T. Lügger, R. Fröhlich, *Eur. J. Inorg. Chem.* **2004**, 394–400.

[12] a) A. K. Boudalis, N. Lalioti, G. A. Spyroulias, C. P. Raptopoulou, A. Terzis, V. Tangoulis, S. P. Perlepes, *J. Chem. Soc., Dalton Trans.* **2001**, 955–957; b) A. K. Boudalis, N. Lalioti, G. A. Spyroulias, C. P. Raptopoulou, A. Terzis, A. Bousseksou, V. Tangoulis, J.-P. Tuchagues, S. P. Perlepes, *Inorg. Chem.* **2002**, *41*, 6474–6487; c) A. K. Boudalis, C. P. Raptopoulou, A. Terzis, S. P. Perlepes, *Polyhedron* **2004**, *23*, 1271–1277; d) A. K. Boudalis, Y. Sanakis, C. P. Raptopoulou, V. Psycharis, A. Terzis, *Polyhedron* **2006**, *25*, 1391–1398; e) A. K. Boudalis, Y. Sanakis, C. P. Raptopoulou, V. Psycharis, *Inorg. Chim. Acta* **2007**, *360*, 39–47.

[13] a) C. Gkioni, A. K. Boudalis, Y. Sanakis, C. P. Raptopoulou, *Polyhedron* **2007**, *26*, 2536–2542; b) K. N. Lazarou, I. Chadjistamatis, V. Psycharis, S. P. Perlepes, C. P. Raptopoulou, *Inorg. Chem. Commun.* **2007**, *10*, 318–323.

[14] a) M. Mikuriya, T. Kotera, F. Adachi, M. Handa, M. Koikawa, H. Okawa, *Bull. Chem. Soc. Jpn.* **1995**, *68*, 574–580; b) H. Nasri, M. K. Ellison, B. Shaevitz, G. P. Gupta, W. R. Sheidt, *Inorg. Chem.* **2006**, *45*, 5284–5290.

[15] M. Tiliakos, P. Cordopatis, A. Terzis, C. P. Raptopoulou, S. P. Perlepes, E. Manessi-Zoupa, *Polyhedron* **2001**, *20*, 2203–2214.

[16] C. P. Raptopoulou, unpublished results.

[17] C. P. Raptopoulou, V. Tangoulis, E. Devlin, *Angew. Chem. Int. Ed.* **2002**, *41*, 2386–2389.

[18] Mössbauer spectra of powder samples of the orange and dark-blue precipitates were recorded at 78K. The spectrum of the orange precipitate was simulated by assuming two quadrupole-split doublets. The major species (ca. 95% of total iron) exhibits $\delta = 0.50(\pm0.01)$ mm s^{-1} and $\Delta E_Q = 2.10(\pm0.01)$ mm s^{-1} and is consistent with a Fe^{III}–O–Fe^{III} dimer. The minor species (ca. 5% of total iron) exhibits $\delta = 0.53(\pm0.02)$ mm s^{-1} and $\Delta E_Q = 0.62(\pm0.02)$ mm s^{-1} and is attributed to a monomeric high-spin Fe^{III} complex. The spectrum of the dark-blue precipitate exhibits a relatively narrow quadrupole-split doublet with $\delta = 0.28(\pm0.01)$ mm s^{-1} and $\Delta E_Q = 1.01(\pm0.01)$ mm s^{-1}, consistent with a low-spin Fe^{II} complex. At room temperature, this sample exhibits a doublet, which is also consistent with low-spin Fe^{II}. The Mössbauer parameters from the orange and dark-blue precipitates are in agreement with the corresponding values for **2** and **3**, respectively.
[19] a) L. Chafetz, *J. Pharm. Sci.* **1964**, *53*, 1192–1196; b) S. B. Hanna, S. A. Sarac, *J. Org. Chem.* **1977**, *42*, 2063–2068.
[20] O. Scialdone, M. A. Sabatino, C. Belfiorez, A. Galia, M. P. Paternostro, G. Filardo, *Electrochim. Acta* **2006**, *51*, 3500–3505.
[21] In acidic aqueous solutions the standard reduction potential rises from +0.77 V for the $[Fe(H_2O)_6]^{2+/3+}$ redox couple to +1.12 V for $[Fe(phen)_3]^{3+/2+}$. See: F. A. Cotton, G. Wilkinson, *Advanced Inorganic Chemistry*, 4th ed., John Wiley & Sons, New York, **1980**.
[22] a) I. Morgenstern-Badarau, F. Lambert, J.-P. Renault, M. Cesario, J.-D. Maréchal, F. Maseras, *Inorg. Chim. Acta* **2000**, *297*, 338–350; b) G. Brewer, C. Luckett, L. May, A. M. Beatty, W. R. Scheidt, *Inorg. Chim. Acta* **2004**, *357*, 2390–2396; c) M. J. Hardie, C. A. Kilner, M. A. Halcrow, *Acta Crystallogr., Sect. C* **2004**, *60*, m177–m179.
[23] L. J. Bellamy, *The Infrared Spectra of Complex Molecules*, 3rd ed., Chapman and Hall, London, **1975**.
[24] K. Nakamoto, *Infrared and Raman Spectra of Inorganic and Coordination Compounds*, 4th ed., Wiley, New York, **1986**.
[25] J. Sanders-Loehr, W. D. Wheeler, A. K. Shiemke, B. A. Averill, T. M. Loehr, *J. Am. Chem. Soc.* **1989**, *111*, 8084–8093.
[26] a) J. S. Singh, *J. Mol. Struct.* **2008**, *876*, 127–133; b) A. K. Rai, R. Singh, K. N. Singh, V. B. Singh, *Spectrochim. Acta A* **2006**, *63*, 483–490; c) M. Boczar, L. Boda, M. J. Wójcik, *J. Chem. Phys.* **2006**, *125*, 084709–1–084709–13.
[27] D. Wester, G. J. Palenik, *J. Am. Chem. Soc.* **1973**, *95*, 6505–6506.
[28] M. G. B. Drew, A. H. bin Othman, P. McIlroy, S. M. Nelson, *Acta Crystallogr., Sect. B* **1976**, *32*, 1029–1031.
[29] R. Keuleers, G. S. Papaefstathiou, C. P. Raptopoulou, V. Tangoulis, H. O. Desseyn, S. P. Perlepes, *Inorg. Chem. Commun.* **1999**, *2*, 472–475.
[30] H. Zhao, M. Shatruk, A. V. Prosvirin, K. R. Dunbar, *Chem. Eur. J.* **2007**, *13*, 6573–6589.
[31] D.-I. Che, G. Li, B.-S. Du, Z. Zhang, Y.-H. Li, *Inorg. Chim. Acta* **1997**, *261*, 121–127.
[32] S. Hayami, K. Danjobara, Y. Shigeyoshi, K. Inoue, Y. Ogawa, Y. Maeda, *Inorg. Chem. Commun.* **2005**, *8*, 506–509.
[33] E. C. Constable, C. E. Housecroft, M. Neuburger, S. Schaffner, E. J. Shardlow, *Inorg. Chim. Acta* **2007**, *360*, 4069–4076.
[34] L. M. Toma, D. Armentano, G. De Munno, J. Sletten, F. Lloret, M. Julve, *Polyhedron* **2007**, *26*, 5263–5270.
[35] B. Gallois, J.-A. Real, C. Hauw, J. Zarembowitch, *Inorg. Chem.* **1990**, *29*, 1152–1158.
[36] D. C. Figg, R. H. Herber, J. A. Potenza, *Inorg. Chem.* **1992**, *31*, 2111–2117.
[37] a) G. A. Barclay, R. S. Vagg, E. C. Watton, *Acta Crystallogr., Sect. B* **1977**, *33*, 3487–3491; b) P. Byers, G. Y. S. Chan, M. G. B. Drew, M. J. Hudson, C. Madic, *Polyhedron* **1996**, *15*, 2845–2849.
[38] M. A. Harvey, S. Baggio, A. Ibanez, R. Baggio, *Acta Crystallogr., Sect. C* **2004**, *60*, m375-m381.
[39] B. N. Figgis, E. S. Kucharski, S. Mitra, B. W. Skelton, A. H. White, *Aust. J. Chem.* **1990**, *43*, 1269–1276.
[40] R. Zibaseresht, W. T. Robinson, R. M. Hartshorn, *Acta Crystallogr., Sect. E* **2006**, *62*, m1150-m1153.
[41] A. Majumber, G. Pilet, M. Salah El Fallah, J. Ribas, S. Mitra, *Inorg. Chim. Acta* **2007**, *360*, 2307–2312.
[42] N. N. Greenwood, T. C. Gibb, *Mössbauer Spectroscopy*, Chapman and Hall, London, **1971**.
[43] R. Ingalls, *Phys. Rev.* **1964**, *133*, A787-A795.
[44] a) B. W. Fitzsimmons, C. E. Johnson, *Chem. Phys. Lett.* **1974**, *24*, 422–424; b) M. B. O'Donoghue, W. M. Davis, R. R. Schrock, W. M. Reiff, *Inorg. Chem.* **1999**, *38*, 243–252.
[45] a) K. S. Murray, *Coord. Chem. Rev.* **1974**, *12*, 1–35; b) D. M. Kurtz Jr, *Chem. Rev.* **1990**, *90*, 585–606.
[46] A value of 1.12 mm s^{-1} is quoted for the quadrupole splitting for this compound at room temperature. An inspection of Figure 4 of ref.[49] indicates that this value corresponds to $\Delta E_Q/2$.
[47] D. Sedney, M. Kahjehnassiri, W. M. Reiff, *Inorg. Chem.* **1981**, *20*, 3476–3481.
[48] J.-M. Clemente-Juan, C. Mackiewicz, M. Verelst, F. Dahan, A. Bousseksou, Y. Sanakis, J.-P. Tuchagues, *Inorg. Chem.* **2002**, *41*, 1478–1491.
[49] F. James, M. Roos, *Comput. Phys. Commun.* **1975**, *10*, 343–367.
[50] a) J. J. Borrás-Almenar, J. M. Clemente-Juan, E. Coronado, B. S. Tsukerblat, *Inorg. Chem.* **1999**, *38*, 6081–6088; b) J. J. Borrás-Almenar, J. M. Clemente-Juan, E. Coronado, B. S. Tsukerblat, *J. Comput. Chem.* **2001**, *22*, 985–991.
[51] G. M. Sheldrick, *SHELXS-97: Structure Solving Program*, University of Göttingen, Germany, **1997**.
[52] G. M. Sheldrick, *SHELXL-97: Crystal Structure Refinement*, University of Göttingen, Germany, **1997**.

Received: June 2, 2008
Published Online: November 21, 2008

